Journal of Materials Chemistry A

ROYAL SOCIETY OF CHEMISTRY

PAPER

View Article Online
View Journal | View Issue

Cite this: J. Mater. Chem. A, 2024, 12, 28326

Understanding the reaction pathway of lithium borohydride-hydroxide-based multi-component systems for enhanced hydrogen storage†

Sweta Munshi, *[a] Gavin S. Walker, [a] Kandavel Manickam,[a] Thomas Hansen, [b] Martin Dornheim[a] and David M. Grant [a]

Complex hydride–metal hydroxide multicomponent hydrogen storage systems have high potential for hydrogen storage because their dehydrogenation thermodynamics can be tuned while maintaining a high hydrogen storage capacity. Out of all the ratios explored using lithium borohydride and lithium hydroxide ($LiBH_4$–$xLiOH$, $x = 1, 3, 4$), a particularly promising system is $LiBH_4$–3LiOH with a maximum storage capacity of 7.47 wt%. Thermal and diffraction studies along with *in situ* neutron diffraction reveal new insights into the intermediate phases involved in the reaction pathway, enabling the identification of a detailed reaction schematic. The onset decomposition temperature was reduced to 220 °C for the hand-milled 1 : 3 system, releasing 6 wt% of H_2 by 370 °C. Li_3BO_3 was the main decomposition product. Other than a small trace of water, no toxic gas release was detected along with the H_2 release. Ball-milling showed improved reaction kinetics by releasing around 6 wt% between 200 and 260 °C in one step. The destabilization was achieved through the coupling reaction between $H^{\delta-}$ in $[BH_4]^-$ and $H^{\delta+}$ in $[OH]^-$. Among all the catalysts investigated, the addition of 5 wt% $NiCl_2$ led to further improvement in reaction kinetics. This resulted in a decrease in the onset decomposition temperature to 80 °C and released 6 wt% of H_2 below 300 °C. The systems have exhibited improvements in kinetics and operational temperature, showing potential as a single use hydrogen storage material.

Received 1st August 2024
Accepted 10th September 2024

DOI: 10.1039/d4ta05368k

rsc.li/materials-a

1. Introduction

The development of a cost-effective and energy-dense hydrogen storage system with a moderate operating condition is one of the key challenges in the hydrogen economy. Extensive research has explored various materials for hydrogen storage including complex hydrides such as borohydrides $[BH_4]^-$,[1–4] alanates $[AlH_4]^-$[5,6] and amides $[NH_2]$,[7–9] demonstrating promising gravimetric densities. Lithium-based complex hydrides, particularly due to the lightweight of lithium, gathered interest as potential hydrogen storage materials. Lithium borohydride has gained much interest in this field due to its high gravimetric and volumetric hydrogen capacities of 18.5 wt% and 121 kg m^{-3}, respectively.[2] However, they suffer from high thermodynamic stability and slow dehydrogenation kinetics. This necessitates high temperatures, exceeding 400–600°C, for major hydrogen release.[1,2]

In recent studies, several effective methods such as milling,[10–12] catalyst addition[13–15] and nano-confinement[16,17] have been studied to improve the hydrogen storage properties of $LiBH_4$. Among these, the additive-based method is a simple way to tune $LiBH_4$ thermodynamic properties (*i.e.* destabilization).[18] Vajo *et al.*[19] demonstrated the destabilization of $LiBH_4$ by incorporating MgH_2 as an additive, leading to a $2LiBH_4$–MgH_2 composite with a reversible hydrogen capacity of 8–10 wt% and rapid reaction kinetics at moderate temperatures (300–400 °C). Subsequent research led to the development of destabilized $LiBH_4$ composites with enhanced hydrogen properties, including $LiBH_4$–Al/Ni/Ti,[20–22] $LiBH_4$–MgH_2/CaH_2/SrH_2/CeH_2,[22–26] $LiBH_4$–SiO_2/TiO_2/SnO_2,[27–29] and $LiBH_4$–$CaNi_5$.[30] While the additives demonstrably enhance both thermodynamic and kinetic properties of $LiBH_4$, most systems still require decomposition temperatures exceeding 300 °C for major hydrogen release. Therefore, the development of novel lightweight destabilizers capable of catalysing the dehydrogenation of $LiBH_4$ at substantially lower temperatures remains an essential area of investigation.

The $H^{\delta+}/H^{\delta-}$ coupling mechanism proposed by Chen[31] and the development of complexes incorporating both H^+ and H^- were investigated through the reaction of $LiNH_2$ and LiH. In their study, hydrogen release was observed from the mixture $[LiNH_2$–$2LiH]$ at 150 °C, attributed to the reaction between $H^{\delta+}$ in $[NH_2]^-$ and $H^{\delta-}$ in LiH. Since then, numerous research studies have been published based on the H^+/H^- coupling

[a]Advanced Materials Research Group, Faculty of Engineering, University of Nottingham, UK. E-mail: swetamunshi.sm@gmail.com

[b]Institut Laue-Langevin, Grenoble, France

† Electronic supplementary information (ESI) available. See DOI: https://doi.org/10.1039/d4ta05368k

reaction.[32–34] This suggests that alkali metal hydroxides (such as LiOH, NaOH, and KOH) are likely to efficiently destabilize $LiBH_4$ due to the interaction between $H^{\delta+}$ in $[OH]^-$ and $H^{\delta-}$ in $[BH_4]^-$. The absence of B_2H_6 or other toxic gases in the released products, as reported in the literature,[35] along with lithium's lightweight nature and the high hydrogen content of 11 wt% in the $LiBH_4$–LiOH system, makes LiOH a promising additive for $LiBH_4$. Although many studies have focused on $LiBH_4$ hydrolysis in the $LiBH_4$–H_2O system[36–38] which has some similarities with hydroxide systems, the solid–liquid reaction for hydrolysed systems raises significant safety concerns due to the unpredictable generation of hydrogen, as well as issues related to hydrogen efficiency, cost of borohydrides and poor reversibility. Investigating the destabilization of $LiBH_4$ using alkali metal hydroxides in a solid–solid reaction could address many of these challenges, making it an area of considerable interest.

Cai *et al.*[35] identified $LiBH_4$–*x*LiOH as the most favourable system among various hydroxide-based options. The degree of $LiBH_4$ destabilization by alkali metal hydroxides followed the trend LiOH > NaOH > KOH, attributed to the superior acidity of LiOH, due to lithium's highest electronegativity, releasing H_2 at 200 °C for the $LiBH_4$–LiOH system. Vajo *et al.*[39] investigated similar systems and found that LiOH greatly destabilises $LiBH_4$ by releasing hydrogen at 270 °C for the $LiBH_4$–4LiOH composite. Due to magnesium's highest electronegativity, among all the hydroxides explored, $LiBH_4$–*x*$Mg(OH)_2$-based systems showed an onset decomposition at 150 °C.[40] However, the majority of the stored hydrogen was released above 300 °C, making this system unattractive.

The destabilised system $LiBH_4$–*x*LiOH reported by researchers,[35,39] was principally in the stoichiometric ratio of $LiBH_4$–4LiOH, though discrepancies have been noted in the reported results. The variety of reported products resulting from the same additions emphasizes the crucial role of understanding the reaction pathway to identify the behaviour of the system and how to optimise it. Experiments on a 1 : 3 stoichiometry which may offer both improved kinetics and an alternative reaction pathway, have not been investigated. The literature on reported systems illustrates the lack of understanding of the system and the process involved, its behaviour under varying stoichiometry and reaction conditions. For this work, a detailed investigation on $LiBH_4$–*x*LiOH systems was performed, and the stoichiometric ratio and milling treatment were investigated, and the study focused on the $LiBH_4$–3LiOH system which was found to be the optimum stoichiometry. Nickel chloride as a catalyst precursor was investigated to accelerate the dehydrogenation kinetics and *in situ* powder neutron diffraction (PND) was used to investigate the reaction pathway.

2. Experimental

2.1 Materials

$LiBH_4$ (≥95%, Sigma-Aldrich), anhydrous LiOH (≥98%, Sigma-Aldrich), $NiCl_2$ (98%, Sigma-Aldrich), $Li^{11}BD_4$ (^{11}B > 99, *D* > 98, Katchem), D_2O (99.9%, Sigma-Aldrich) and Li_2O (97%, Sigma-Aldrich) were used as received. All samples, except D_2O, were stored and handled in an MBRAUN Unilab argon-filled glove box (oxygen and water levels below 0.1 ppm).

Synthesis of $LiBH_4$–*x*LiOH composites. For most characterisation studies, sample preparation used 0.1 to 0.5 g of material loaded into stainless-steel milling pots containing hardened stainless-steel balls (approximately 4 mm in diameter) with a ball-to-sample weight ratio of 120 : 1. Ball milling was conducted using a Fritsch Rotary P5 under an argon atmosphere. As-received LiOH was pre-milled at 400 rpm for 2 hours to obtain a fine powder. For $LiBH_4$–*x*LiOH ($x = 1, 3, 4$) composites, samples were milled at 200 rpm for 30 minutes.

For the powder neutron diffraction (PND) study, anhydrous litihum deuteroxide (LiOD) was prepared by reacting Li_2O with excess D_2O according to eqn (1) and (2). About 500 mg of Li_2O was slowly added to 1 mL of D_2O in a Schlenk flask under argon flow while continuously stirring. This formed hydrous material, $LiOD \cdot D_2O$, which was then heated at 175 °C for 4 h under vacuum to get rid of all the D_2O.

$$Li_2O + 3D_2O \rightarrow 2LiOD \cdot D_2O \quad (1)$$

$$2LiOD \cdot D_2O \xrightarrow{\Delta} 2LiOD + 2D_2O\uparrow \quad (2)$$

$LiBD_4$–*x*LiOD (x = 1, 3, 4) composites were prepared by initially ball milling prepared LiOD separately for 2 hours to reduce the particle size. The $LiBD_4$-*x*LiOD mixtures were then hand-milled using a mortar and pestle for 15 minutes. This approach was chosen to avoid hydrogen evolution during ball milling and to accommodate the large quantity required for the PND experiment. To facilitate a more accurate comparison with PND data, separate thermal gravimetric analysis (TGA) and temperature programmed desorption – mass spectrometry (TPD-MS) (ESI, ES3†) experiments were conducted using hydride samples prepared under similar milling conditions to the PND samples.

2.2 Characterisation

Thermal gravimetric analysis (TGA) was conducted on a Netzsch 209 F1 instrument under a constant 100 mL min^{-1} argon flow in the temperature range of 30–570 °C and at a heating ramp of 10 °C min^{-1}. The desired amount of sample was placed in alumina crucibles and sealed within an aluminium pan and a lid. The lid was pierced shortly before loading the pan into the instrument.

Temperature programmed desorption – mass spectrometry (TPD-MS) was performed on a Hiden CATLAB microreactor coupled with a mass spectrometer (MS, QIC 20). Around 10 mg of samples were loaded into the sample cell and studied between 30 and –570 °C with a heating ramp of 10 °C min^{-1} under an argon flow of 100 mL min^{-1}.

Ex situ powder X-ray diffraction (XRD) was performed using a DaVinci Bruker D8 Advance with a CuKα source ($\lambda = 1.5418$ Å) in the 2θ range of 10–70°, a step size of 0.02° and a time/step of 0.4 s. Samples were placed on a Si crystal wafer and covered with plastic tape to protect the materials from oxidation.

In situ powder neutron diffraction (PND) measurements were carried out at the Institute Laue–Langevin (ILL) in Grenoble,

France. A D1B neutron diffractometer was used for the $LiBH_4$–3LiOH system ($\lambda = 2.52$ Å). Around 1.5 g of samples were loaded into a 316 L stainless steel vessel under argon. The experiment was performed under a self-generated D_2 atmosphere (initially under a static vacuum). Around 2 g of sample was heated up to 570 °C, starting at 50 °C with a heating ramp of 1 °C min^{-1} and data were collected in 5 min time intervals. Data analysis was performed on the Large Array Manipulation Program (LAMP), designed by ILL.

Diffuse reflectance infra-red Fourier transform spectroscopy (DRIFTS) was carried out on a Bruker IFS 66/S using a sealed Pike environment cell (HC-900). Samples were mixed with potassium bromide in 1 : 10 ratio using a mortar and pestle in an argon-filled glove box. The sample was then loaded into a crucible and sealed inside the environment cell. The samples were heated internally with a temperature controller. The spectra were recorded with a resolution of 8 cm^{-1} after a KBr background scan had been recorded for the same resolution.

3. Results and discussion

3.1 The effect of stoichiometry on the interaction between $[BH_4]^-$ and $[OH]^-$

The decomposition behaviour of $LiBH_4$–xLiOH (x = 1, 3, 4) composites is illustrated in Fig. 1. Upon heating as-received $LiBH_4$, material decomposition starts at 270 °C, with main decomposition starting above 380 °C and reaching up to 12 wt% by 570 °C, consistent with previous findings.[1,2,19] Conversely, the thermal decomposition of LiOH starts at 450 °C, releasing H_2O, and reaches about 11 wt% by 570 °C.[41] For $LiBH_4$–LiOH, the incorporation of LiOH notably reduces the operating temperature required for hydrogen desorption from $LiBH_4$. It should be noted that hydrogen desorption from $LiBH_4$–LiOH composite exhibits multistep reaction characteristics within the temperature range of 175–450 °C, which is obviously different from the pristine $LiBH_4$. This phenomenon suggests that the presence of LiOH changes the dehydrogenation reaction mechanism of $LiBH_4$, *viz.*, there is a chemical reaction between $LiBH_4$ and LiOH. Initially, as the temperature increases, approximately 4 wt% of hydrogen is released between 170 to 270 °C. Subsequently, between 350 and –450 °C, an additional H_2 release of 2.6 wt% was observed, followed by a further 0.9 wt% liberated upon heating beyond 500 °C. By 570 °C, a total mass loss of approximately 7.5 wt% is observed for the 1 : 1 system out of a theoretical hydrogen storage capacity of 10.9 wt%, indicating that the observed mass loss may primarily result from hydrogen loss. Considering all weight loss corresponds solely to hydrogen, the weight loss corresponds to 68.6% of the total hydrogen, equivalent to 3.4H. To influence the reaction pathway further by increasing the amount of LiOH from 1 mol to 3 mol in $LiBH_4$–xLiOH composites, a gradual high-temperature shift in the dehydrogenation curves is observed, accompanied by a significant increase in the dehydrogenation amount at lower temperatures. In the non-isothermal experiment, a total mass loss of slightly more than 6 wt% is observed within the temperature range of 220 to 260 °C, out of a theoretical hydrogen storage capacity of 7.47 wt%, corresponding to 80.8% of the total hydrogen, *i.e.*, 5.6H. Increase of the added amount of LiOH to the ratio of 1 : 4, resulted in a notable decrease in the dehydrogenation quantity in the low temperature regime when compared to the 1 : 3 system. A significant increase in the dehydrogenation temperature was observed. The $LiBH_4$–4LiOH system showed three-step decomposition starting at 230–280 °C, 320–400 °C and a large mass loss step at temperature above 430 °C. The major decomposition for this system was observed at 230 °C, losing around 4.2 wt% by 300 °C. Another small weight loss was observed above 330 °C, losing around 0.7 wt% by 380 °C. Post 440 °C, a big drop in weight could be seen of around 5.6 wt%, continued till 570 °C. Interestingly, a total of around 11.1 wt% mass loss was observed for the 1 : 4 system out of 6.85 wt% theoretical hydrogen storage capacity which indicates the release of side products along with H_2.

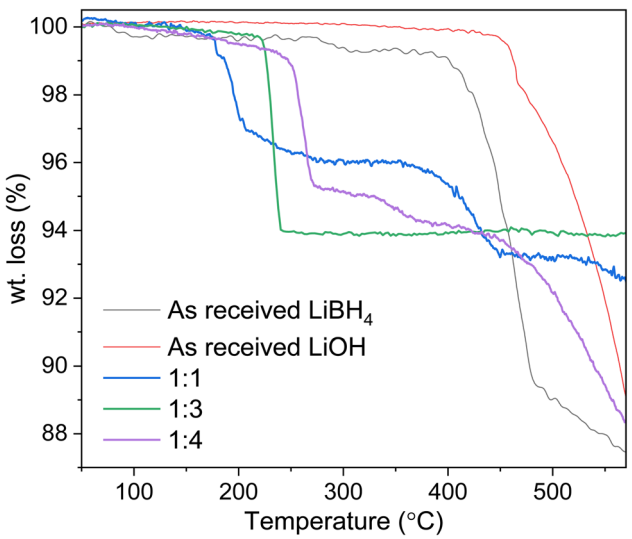

Fig. 1 Summarised TGA data for as-received reactants ($LiBH_4$ and LiOH) and $LiBH_4$–xLiOH (x = 1, 3, 4) composites studied on heating to 570 °C at 10 °C min^{-1} under argon flow.

Fig. 2 shows the TPD-MS curves of the $LiBH_4$–xLiOH (x = 1, 3, 4) composites. It is evident from the curves that mostly the H_2 signal was observed during heating from room temperature to 570 °C for all composites, with only a minimal presence of H_2O. Thus, it can be inferred that the gas released from the $LiBH_4$–xLiOH (x = 1, 3, 4) composites upon heating is predominantly hydrogen. In the TPD-MS curve for the 1 : 1 system, five distinct dehydrogenation peaks are observed, providing compelling evidence for a stepwise dehydrogenation process. The peak temperatures for hydrogen desorption from the $LiBH_4$–LiOH composite are measured to be 170, 200, 235, 422, and 540 °C. These temperatures are in good agreement with the results depicted in Fig. 1. Furthermore, an increase in the LiOH content in $LiBH_4$–xLiOH composites causes the dehydrogenation peak to shift from 170 to 220 °C. Interestingly, for 1 : 3 composites, most of the stored hydrogen was liberated below 300 °C, a temperature below the melting point of $LiBH_4$. No further weight loss or hydrogen release was discernible for the 1 : 3 system in Fig. 1 and 2. Conversely, for the 1 : 4 composite, a three-step hydrogen release profile was evident, consistent

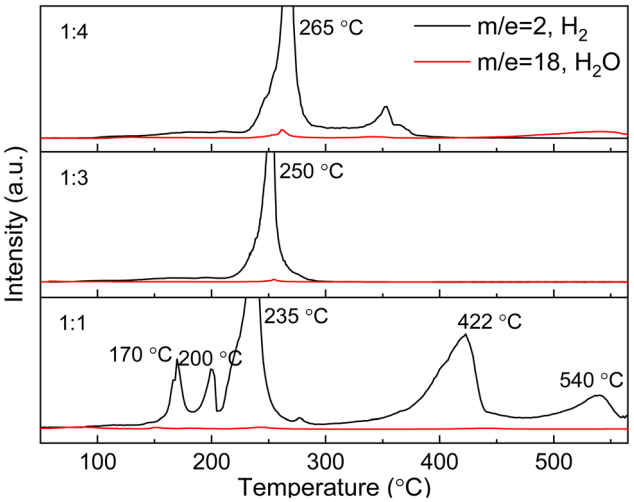

Fig. 2 Summarised TPD-MS data for $LiBH_4$–xLiOH (x = 1, 3, 4) composites studied on heating to 570 °C at 10 °C min^{-1} under argon flow.

with observations in Fig. 1. Notably, a prominent H_2O peak emerged for the 1 : 4 composite above 450 °C, indicating that the weight loss at this stage was attributable to the release of H_2O from the system which justifies 11.1 wt% loss from the system.

Further insights into the decomposition process are provided by the FTIR profile of $LiBH_4$–xLiOH (x = 1, 3, 4) composites (Fig. 3). A notable decrease in O–H stretching band (3500–3700 cm^{-1}) intensity is noted for the 1 : 1 composite, as the system undergoes heating from 25 °C to 300 °C,[35,42] while there is minimal alteration in bands corresponding to B–H bending (1100 cm^{-1}) and B–H stretching (2200–2500 cm^{-1}).[42] This implies that the weight loss observed during the initial dehydrogenation step below 300 °C is attributed to interactions between $[BH_4]^-$ and $[OH]^-$ units, with most of the LiOH being consumed in this process, while the system remains rich in $LiBH_4$. As the temperature increased up to 450 °C, the intensity of the B–H band gradually decreased, indicating that the second phase of weight loss observed in the TGA profile for the 1 : 1 composite post 350 °C arises from the decomposition of excess $LiBH_4$ after this temperature threshold, thereby signifying the $LiBH_4$ rich nature of this system. The FTIR profile for the 1 : 3 composite shows a significant reduction in the intensity of O–H and B–H stretching bands when the system is heated from 25 °C to 300 °C, which demonstrates that the liberation of H_2 was due to the occurrence of the reaction between $H^{\delta+}$ in $[OH]^-$ and $H^{\delta-}$ in $[BH_4]^-$ at this stage.

The FTIR profile for the $LiBH_4$–4LiOH system shows a significant reduction in the B–H band compared to O–H when heated to 300 °C. The IR data showed a weak B–H band at 300 °C which was no longer visible at 450 °C but was replaced by two small peaks at similar positions. The appearance of these two small peaks at 2200 and 2500 cm^{-1} is attributed to different B–H stretching in a *closo*-dodecaborane Li–B–H cluster coming from $LiBH_4$ decomposition intermediate $Li_xB_yH_z$ post 320 °C,[43,44] which supports the weight loss occurring at the second stage (320–400 °C) in Fig. 1. The third step after 430 °C showed a major weight loss of around 5.6 wt% and was due to H_2O release. This is supported by the FTIR spectrum at 450 °C showing the continued presence of the O–H band. Hence, the third step is the thermal decomposition of the remaining LiOH following eqn (3), *i.e.* for the 1 : 4 system the LiOH was in excess.[41]

$$LiOH \rightarrow \frac{1}{2}Li_2O + \frac{1}{2}H_2O \quad (3)$$

Considering both the dehydrogenation temperature and hydrogen capacity, the optimal system is determined to be $LiBH_4$–3LiOH in this case. To further investigate the reaction mechanism of the $LiBH_4$–xLiOH systems, XRD was employed. Fig. 4 (i) shows the XRD patterns for the $LiBH_4$–xLiOH system at room temperature after milling and (ii) after dehydrogenation. The post-milled XRD pattern displayed prominent peaks corresponding to the starting materials, $LiBH_4$ [ICDD pdf card no. 01-070-9017] and LiOH [ICDD card no. 00-032-0564]. XRD analysis of the post-milled sample at room temperature revealed peaks characteristic of a new unknown phase, termed the 1st intermediate phase. When the XRD profile was examined at 570 °C, distinct and strong peaks of the final product, Li_3BO_3 [ICDD card no. 00-018-0718], were observed, while no peaks from $LiBH_4$ or the 1st intermediate were visible. The presence of the B–O stretching bands at 1260 cm^{-1} and 1460 cm^{-1}, indicative of the BO_3 unit,[45,46] became evident in the FTIR profile after reaching 300 °C (Fig. 3), providing additional

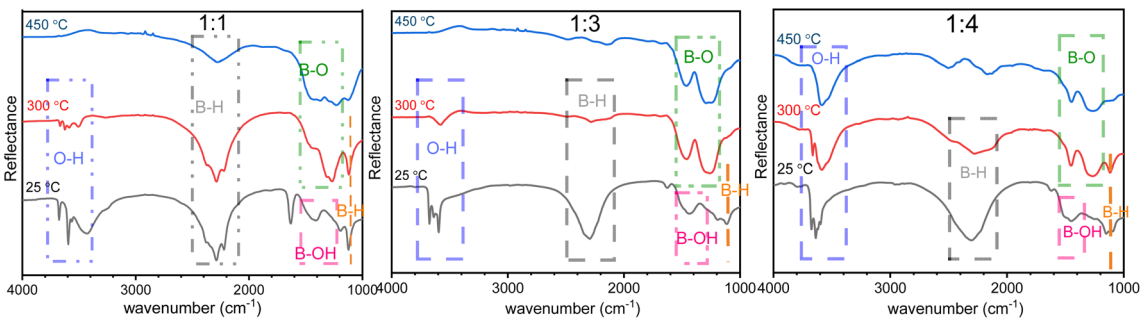

Fig. 3 FTIR data for $LiBH_4$–xLiOH (x = 1, 3, 4) composites upon heating up to 450 °C.

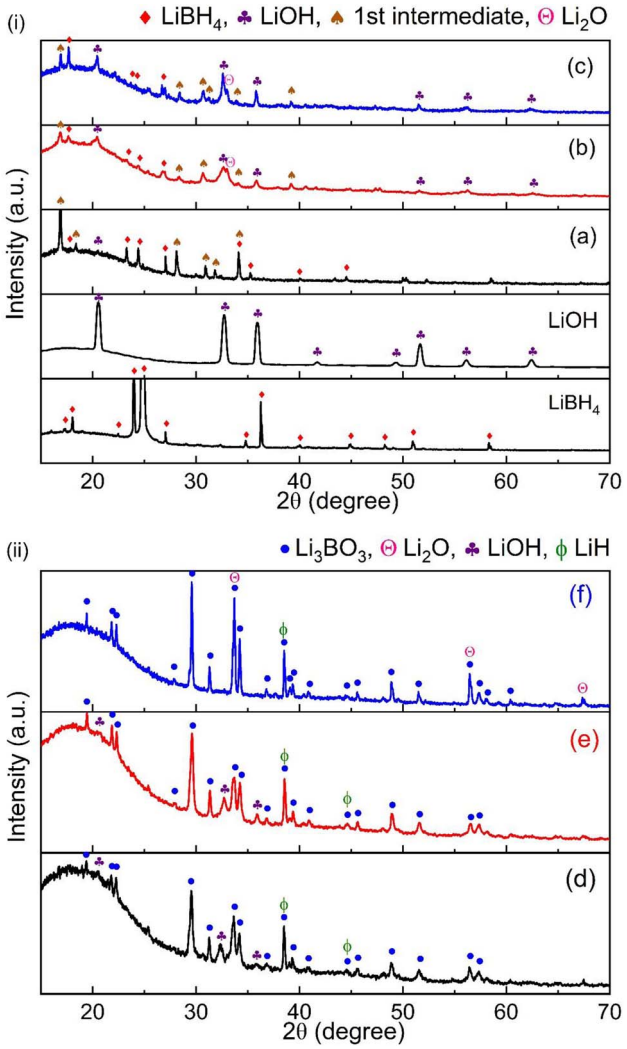

Fig. 4 (i) XRD patterns of post-milled room temperature $LiBH_4$–xLiOH (x = 1, 3, 4) composites – (a) 1 : 1, (b) 1 : 3, (c) 1 : 4, and (ii) post decomposition pattern at 570 °C – (d) 1 : 1, (e) 1 : 3, and (f) 1 : 4.

confirmation for the formation of Li_3BO_3. Moreover, the presence of the LiH phase was also identified in dehydrogenated samples. For the 1 : 4 system, strong presence of Li_2O was detected which supports LiOH decomposition post 450 °C, following eqn (3). The appearance of LiOH peaks in the dehydrogenated 1 : 1 and 1 : 3 samples might result from the substantial presence of LiH in these dehydrogenated samples.[47] Exposure to moisture during the transfer process for XRD measurement allows LiH to react with the moisture, forming LiOH. Based on TG/IR/XRD results, the overall reaction for 1 : 1, 1 : 3 and 1 : 4 systems is as given below.

$$LiBH_4 + LiOH \xrightarrow{570\ ^\circ C} kLi_3BO_3 + (1-x)LiBH_4 + zLiH + cB + aH_2 \quad (4)$$

$$LiBH_4 + 3LiOH \xrightarrow{570\ ^\circ C} Li_3BO_3 + LiH + 3H_2 \quad (5)$$

$$LiBH_4 + 4LiOH \xrightarrow{570\ ^\circ C} kLi_3BO_3 + lLi_2O + zLiH + aH_2 + cB + bH_2O \quad (6)$$

3.2 Inclusion of nickel chloride in the $LiBH_4$–3LiOH composite

The optimal stoichiometry from the work above was the $LiBH_4$–3LiOH system. The effect of a catalyst on this system was studied by incorporating $NiCl_2$ to enhance reaction kinetics. TGA/TPD-MS decomposition data for 5 wt% $NiCl_2$ added $LiBH_4$: 3LiOH system are given in Fig. 5, showing a reduction in the decomposition temperature. Starting at 80 °C, a total of 6 wt% mass loss was observed by 300 °C with most of it released at T < 200 °C for the $NiCl_2$ catalysed composite (out of a 7.1 wt% theoretical storage capacity). Total weight loss corresponds to 84.5% of the total hydrogen, *i.e.* 5.9H for the $NiCl_2$ catalysed system. A small weight loss of 0.7 wt% above 400 °C was also observed by the end of the experiment. The reason behind the catalytic activity from the addition of $NiCl_2$ could be due to forming Ni/Ni–B compounds after reacting with $LiBH_4$, starting at 80 °C (ESI, ES3†). The process involves, $LiBH_4$ reacting with $NiCl_2$ to form Ni/Ni–B, LiCl and release H_2.[48,49] These compounds likely aid in activating the B–H bond within the material, thereby reducing the reaction kinetic barrier. The TPD-MS profile reveals two H_2 peaks at 80 °C and 150 °C. The first peak results from the $LiBH_4$–$NiCl_2$ reaction (Fig. 5), while the second peak is due to the formed Ni/Ni–B acting as a catalyst to facilitate the $H^+ \ldots H^-$ reaction in $[BH_4]^-$ – $[OH]^-$.

3.3 Reaction mechanism for the $LiBH_4$–xLiOH composite

Given the excellent results obtained with the $LiBH_4$–xLiOH composite, additional investigations into these composites were necessary to fully understand the reaction mechanism. Fig. 6 shows the *in situ* PND profile for the $LiBD_4$–3LiOD system. The presence of Li_2O contamination in the prepared LiOD

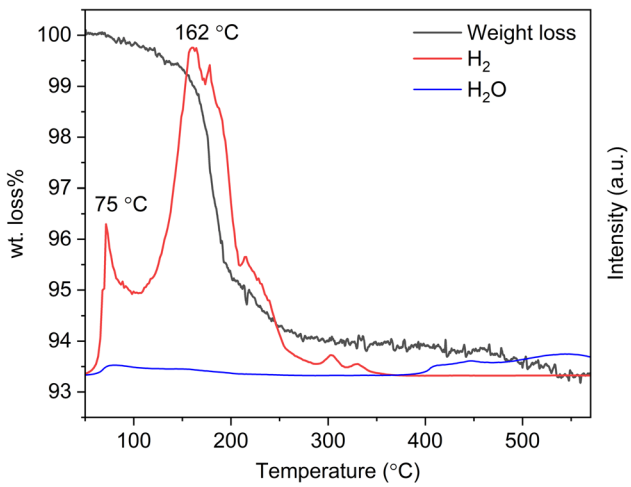

Fig. 5 TGA-TPD-MS data for $LiBH_4$–3LiOH-5 wt% $NiCl_2$ doped systems heated to 570 °C at 10 °C min^{-1} under Ar flow.

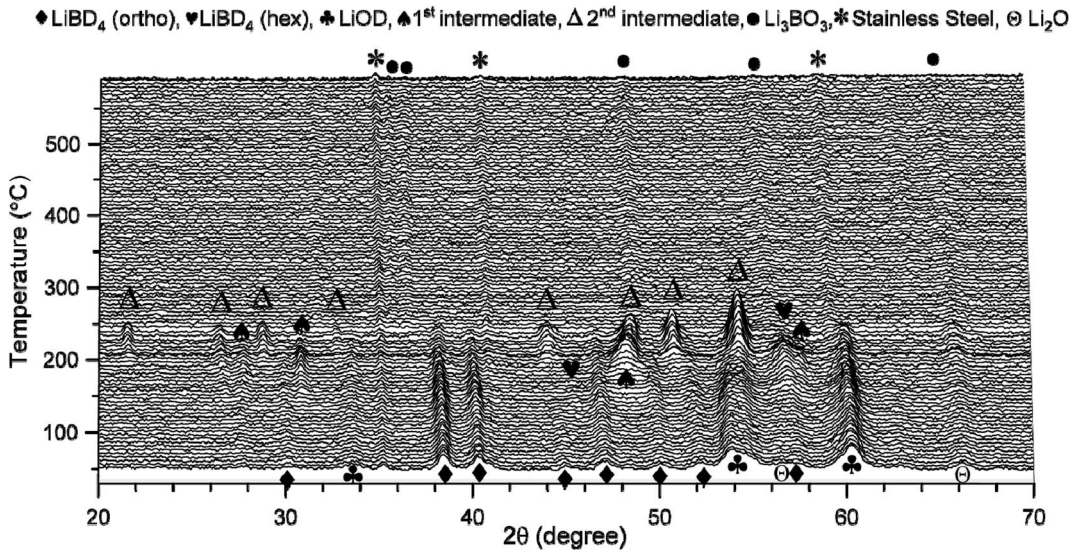

Fig. 6 PND profile for $LiBD_4$–3LiOD on heating to 570 °C at 1 °C min^{-1} under a self-generated D_2 atmosphere ($\lambda = 2.52$ Å).[50]

sample resulted in the observed Li_2O peaks in the starting material.

Due to the complexity of the overall 3D plot, it was challenging to understand the occurrence of phase changes and the products generated along with changes in temperature. Therefore, separate intensity profiles were created for each phase to understand the progress of the reaction throughout the decomposition process (Fig. 7).

A reminder that the PND samples were hand-milled, separate TGA and TPD-MS results of these samples are given in ESI, ES3.† At the start of the NPD experiment, intense peaks of starting materials, $LiBD_4$ and LiOD were observed. Two peaks from Li_2O were also observed at room temperature owing to unreacted oxide in the prepared LiOD. At above 120 °C, the intensity of the reactants $LiBD_4$ and LiOD started to decrease, and the peaks completely disappeared at 220 °C. Besides the reactant phases, the presence of a weak peak at 28° (2θ) at room temperature was attributed to the formation of the 1st intermediate, also evident in the XRD profile (Fig. 4). This peak continued to grow until 180 °C, accompanied by other peaks associated with the 1st intermediate at 30.1°, 47.5° and 57.7° in 2θ, which began to appear after 150 °C. The diffraction pattern for the 1st intermediate matches closely with lithium tetrahydroxyborate, $LiB(OH)_4$ [ICDD: 00-044-0419], but will be the deuterated analogue, $LiB(OD)_4$. The formation of the $LiB(OH)_4$ phase can be evidenced from the peak at 1427 cm^{-1} assigned to B–OH bonds appearing below 100 °C in the FTIR spectrum of $LiBH_4$–xLiOH composites (Fig. 3).[51] Fig. 7 displays the PND profile for $LiB(OH)_4$ (decomposed at 180 °C), which is in agreement with the observations by Betourne *et al.*[52] The formation of $LiB(OD)_4$ occurred due to reaction between $[BH_4]^-$ and $[OH]^-$ where $[OH]^-$ replaced H in $[BH_4]^-$ *via* a nucleophilic reaction following short-living intermediates in the order of $BH_3OH^- > BH_2(OH)_2^- > BH(OH)_3^- > B(OH)_4^-$.[53] A plausible reaction for the formation of $LiB(OD)_4$ is presented in eqn (7) and the mechanism presented in Fig. 8. This indicates the occurrence of a reaction at a temperature below 200 °C.

$$0.05LiBH_4 + 0.2LiOH \rightarrow 0.05LiB(OH)_4 + 0.2LiH \quad (7)$$

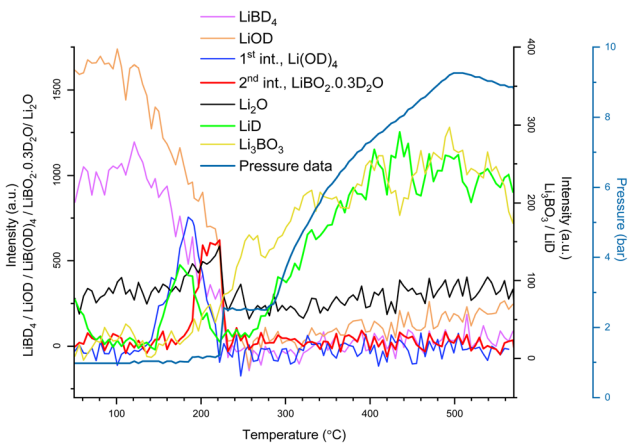

Fig. 7 Peak intensity profile for different species observed during the PND experiment for the $LiBD_4$–3LiOD system upon heating to 570 °C.

In addition, the appearance of the LiD peak in the same temperature range (Fig. 6 and 7) as to the formation of $LiB(OD)_4$ further supports the proposed reaction in eqn (7). A similar intermediate was also reported by DEMİRCİ *et al.*[36] and Goudon *et al.*[37] during a borohydride hydrolysis reaction, which follows a similar reaction mechanism. The appearance of the $LiB(OD)_4$/$LiB(OH)_4$ phase in our post-milled sample suggests that the formation of this intermediate may have started during the milling process.

Post 180 °C, with decreasing intensity of $LiB(OD)_4$ along with the reactants, a new pattern emerged, identified as the 2nd intermediate, in the PND pattern (Fig. 6 and 7). The PND pattern for this phase closely matches with the reported pattern of

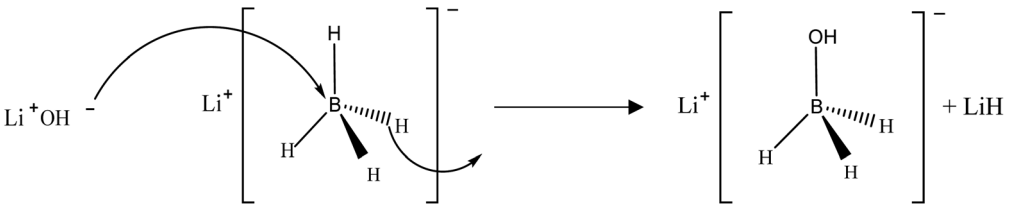

Fig. 8 Nucleophilic substitution reaction between $[BH_4]^-$ and $[OH]^-$.

hydrated lithium borate (*i.e.* $LiBO_2 \cdot 0.3H_2O$) by Koga *et al.*,[54] that is $LiBO_2 \cdot 0.3D_2O$ for this PND experiment. Above 180 °C, $LiB(OD)_4$ decomposes to form hydrated $LiBO_2$ and releases H_2O. A plausible reaction for $LiBO_2 \cdot 0.3D_2O$ formation is proposed in eqn (8).[38,52]

$$0.05LiB(OH)_4 \rightarrow 0.05LiBO_2 \cdot 0.3H_2O + 0.08H_2O \quad (8)$$

The released H_2O can react with LiD to form Li_2O and release H_2 as evident with an increase and decrease in the peak intensities of Li_2O and LiD after 180 °C, respectively (Fig. 7); the reaction mechanism is presented in eqn (9). It is established that when a sub-stoichiometric amount of water is present only to interact with a single surface layer of LiH, Li_2O forms.[47,55] This reaction involves the release of H_2 from the system, supported by a small increase in pressure observed in the PND pressure profile (Fig. 7). This also shows that only a small portion of reactants participate in this reaction mechanism, which did not significantly contribute to the increase in pressure, indicating that it is a side reaction. To further strengthen this argument, TGA and TPD-MS results for hand-milled $LiBH_4$–3LiOH were analysed, ES3 (ESI).† At above 180 °C, the TGA results indicate a minor mass loss of around 0.2 wt% with corresponding results from TPD-MS, showing a broad H_2 peak within the same temperature region. These findings provide further support to $LiB(OH)_4$ decomposition above 180 °C. The stoichiometry of these side reactions, derived from the TG weight loss data, is presented below.

$$0.17LiH + 0.08H_2O \rightarrow 0.08Li_2O + 0.17H_2 \quad (9)$$

At temperatures >220 °C, the peak intensities of the $LiBD_4$/$LiOD$/$LiBO_2 \cdot 0.3H_2O$ phases were drastically reduced and subsequently disappeared (Fig. 6 and 7). This stage is also accompanied by a small pressure rise of up to 1.5 bar in the PND pressure profile. These results are aligned with the TGA results, showing a mass loss of around 0.7 wt% by 270 °C, starting at 220 °C (ESI, ES3†). The TPD-MS profile showed two small peaks of H_2 in the same temperature region, confirming that the weight loss was due to H_2 release from the system and occurred in two steps. This could be due to some of the activated $LiBH_4$ and LiOH reacting *via* the $H^{\delta+}$–$H^{\delta-}$ coupling reaction in 1 : 3 ratio to release H_2. The stoichiometric reaction based on TGA weight loss is stated in eqn (10) and described in Fig. 9. Another small step of weight loss observed above 255 °C was due to $LiBO_2 \cdot 0.3D_2O$ decomposition following eqn (11) (ref. 56) forming dehydrated amorphous $LiBO_2$. The presence of a shoulder in the TGA data above 250 °C, accompanied by the emergence of a small H_2 peak in the TPD-MS profile, provides additional support for the argument. No appearance of $LiBO_2$ post 250 °C along with the disappearance of Li_2O suggested that Li_2O reacted with $LiBO_2$ to form the high temperature stable borate, Li_3BO_3, following eqn (12). This can be also explained with the $Li_2O \cdot B_2O_3$ binary phase diagram.[57] Within the Li_2O–B_2O_3 system, multiple distinct phases can exist at different temperatures based on reactant stoichiometry, such as $LiBO_2$, Li_3BO_3, $Li_2B_4O_7$, $Li_4B_2O_5$ and several others. Given the reaction conditions and dominance of Li_3BO_3 as the main reaction product, support $LiBO_2$ takes up Li_2O to form Li_3BO_3.

$$0.1LiBH_4 + 0.3LiOH \rightarrow 0.1Li_3BO_3 + 0.1LiH + 0.3H_2 \quad (10)$$

$$0.05LiBO_2 \cdot 0.3H_2O \rightarrow 0.05LiBO_2 + 0.01H_2O \quad (11)$$

$$0.05LiBO_2 + 0.05Li_2O \rightarrow 0.05Li_3BO_3 \quad (12)$$

Upon heating above 270 °C, a noticeable rise in pressure data was observed from Fig. 7 along with increasing intensity of Li_3BO_3 and LiD while all the other phases disappeared. The growth of these two phases persisted until the completion of the reaction, indicating their status as primary products. This conclusion is further supported by post-decomposition XRD data for the $LiBH_4$–3LiOH system (Fig. 4). To understand the reaction better, the TGA and TPD-MS data (ESI, ES3†) for hand-milled hydride system were examined. The TGA showed, starting at 270 °C, a large mass loss of around 5.3 wt% by 400 °C, also supported by TPD-MS data, showing an intense peak of H_2 over that temperature range. The H_2 release was driven by the remaining $LiBH_4$ and LiOH reacting *via* the $H^{\delta+}$ – $H^{\delta-}$ coupling reaction in 1 : 3 ratio to release H_2, following eqn (13) and the schematic shown in Fig. 9, also identified as the main decomposition step. The weight loss observed from TGA (ESI, ES3†) data in the main dehydrogenation step corresponds to 70.9% of the total hydrogen *i.e.*, 5H.

$$0.84LiBH_4 + 2.5LiOH \rightarrow 0.84Li_3BO_3 + 0.84LiH + 2.5H_2 \quad (13)$$

No significant changes were observed above 400 °C, except for a minor peak of H_2 detected in the TPD-MS data.

Based on observations, the postulated overall reaction is given below which agrees with the observed results.

$$LiBH_4 + 3LiOH \rightarrow 0.99Li_3BO_3 + 0.96LiH + 0.04Li_2O + 3.02H_2 \quad (14)$$

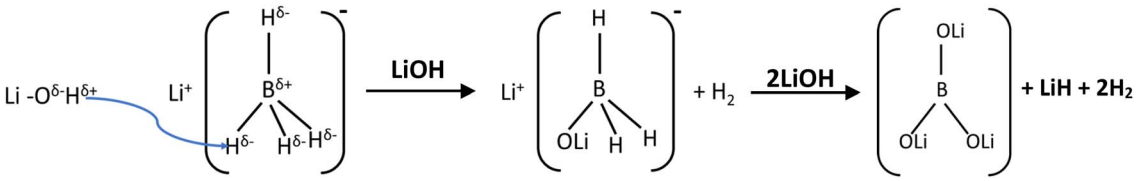

Fig. 9 Coupling reaction mechanism between $H^{\delta+}$–$H^{\delta-}$ in the $[BH_4]^-$/$[OH]^-$ unit.

Table 1 Comparison of the systems for thermodynamic turning of $LiBH_4$

System parameter	Gravimetric capacity (wt%)	Gravimetric capacity (wt%) in solid state (<300 °C)	Decomposition temperature (°C)	Decomposition enthalpy (KJ mol^{-1} H_2)	Hydrogenation condition	Ref.
$LiBH_4$–3LiOH	7.47	6	220–250	−30	—	This work
2$LiBH_4$–MgH_2	10	9.2	270–585	+49	450 °C/24 bar	58 and 59
6$LiBH_4$–CeH_2	7.4	6.1	180–430	+58	350 °C/10 bar	23 and 60
6$LiBH_4$–CaH_2	11.7	9	400–500	+60	450 °C/80 bar	61 and 62
6$LiBH_4$–SrH_2	9.1	8.7	217–500	+48	450 °C/80 bar	24

A point to note is that a significant change in reaction kinetics was observed for the ball-milled (Fig. 1) and hand-milled (ESI, ES3†) $LiBH_4$–3LiOH systems. Starting at 220 °C, most of the stored hydrogen was released by 260 °C when the ball-milled sample was examined. Based on the results observed it can be concluded that milling effectively enhanced the homogeneity of mixing, which influenced the $H^{\delta+}$–$H^{\delta-}$ reaction in $[BH_4]^-$/$[OH]^-$ by bringing them to closer proximity and promoting a single-step hydrogen desorption reaction, while also limiting side reactions temperature below 200 °C.

According to the reaction for the $LiBH_4$–3LiOH system, the reaction pathway for other $LiBH_4$–xLiOH composites becomes evident. In the $LiBH_4$–LiOH system, an abundance of $LiBH_4$ is observed, with surplus $LiBH_4$ undergoing decomposition above 350 °C, as indicated in Fig. 1. The multistep hydrogen release below 300 °C for this system can be attributed to the occurrence of side reactions at lower temperatures. These include the decomposition of $LiB(OH)_4$ after 170 °C, the reaction of excess $LiBH_4$ with released H_2O (200 °C), and the subsequent coupling reaction between $LiBH_4$ and LiOH (230 °C) in Fig. 2. Conversely, in the $LiBH_4$–4LiOH system, an excess of LiOH is present, with additional LiOH decomposing beyond 450 °C, also illustrated in Fig. 1. This proposition finds further support in the TPD-MS/FTIR (Fig. 2 and 3) profile. Moreover, it can be inferred that systems with a higher ratio of LiOH in $LiBH_4$–xLiOH ($x = 3, 4$) effectively suppressed the occurrence of the reaction leading to $LiB(OH)_4$ formation. Conversely, in the $LiBH_4$–LiOH system, the limited availability of LiOH influenced the reaction of $LiB(OH)_4$ formation, evidenced by the strong appearance of $LiB(OH)_4$ in the post-milled XRD profile for the $LiBH_4$–LiOH system (Fig. 4).

4. Summary

The outcomes have exhibited improvements in kinetics and operational temperature, which holds potential for further development in technologies such as stationary hydrogen storage or portable hydrogen storage devices, in applications such as military use. The only by-product generated is a minimal amount of water, enabling the direct utilization of the produced gas in PEMFCs without the need for complex purification processes. Unfortunately, due to the exothermic nature (enthalpy of reaction −30 kJ mol^{-1} of H_2) of the $LiBH_4$–3LiOH system (ES1, ESI†), which shows poor reversibility, efforts are underway to improve its performance. Table 1 below summarises optimally configured systems investigated in this study, compared with some reported studies that demonstrate superior decomposition characteristics compared to most reported $LiBH_4$-binary hydride systems.

5. Conclusion

These results present the first detailed investigation of the $LiBH_4$: xLiOH systems, exploring phase progression, stoichiometry, reaction environment and effect of doping. The robust affinity between $H^{\delta-}$ in $LiBH_4$ and $H^{\delta+}$ in LiOH serves as the driving force for hydrogen desorption from this system. The presence of the hydroxide group, $[OH]^-$, demonstrated a more effective destabilization effect compared to numerous $LiBH_4$-metal hydride systems. The dehydrogenation temperature for $LiBH_4$–LiOH, $LiBH_4$–3LiOH, and $LiBH_4$–4LiOH decreased to 170 °C, 220 °C, and 230 °C, respectively and showed faster kinetics compared to pristine $LiBH_4$. The results suggested the reaction was dependent on the $[BH_4]^-$: $[OH]^-$ ratio. As the $[OH]^-$ content increases, the dehydrogenation temperature also increases incrementally. This suggests a varying interaction between $[BH_4]^-$ and $[OH]^-$ based on their stoichiometry. In the case of $LiBH_4$–LiOH, one $[OH]^-$ reacts with $[BH_4]^-$ which facilitates the liberation of H_2 at a lower temperature. The limited availability of LiOH in the $LiBH_4$–LiOH system indeed favours a nucleophilic reaction mechanism where the oxygen atom in the hydroxide (OH^-) group attacks the boron–hydrogen (B–H) bond, resulting in the formation of the tetrahydroxyborate ion, $B(OH)_4^-$. This process follows a series of short-lived intermediates in the order: $BH_3OH^- \rightarrow BH_2(OH)_2^- \rightarrow BH(OH)_3^- \rightarrow B(OH)_4^-$. However, in

systems with higher LiOH ratios, such as $LiBH_4$–xLiOH ($x = 3, 4$), the interaction between $[BH_4]^-$ and $[OH]^-$ stabilizes $[BH_4]^-$, leading to an observed increase in the dehydrogenation temperature. The higher concentration of LiOH in the milling pot likely alters the chemical environment, facilitating a different mechanism. To explore this further, the reaction mechanism has been studied and is discussed below. Specifically, the excess LiOH may reduce the distance between hydrogen cations (H^+) and hydride anions (H^-), stabilizing the system and favouring the coupling of H^+ and H^- to form hydrogen gas. This H^+–H^- coupling reaction becomes more prominent at temperatures above 200 °C, as observed in the $LiBH_4$–xLiOH ($x = 3, 4$) systems. The primary decomposition product for all systems was Li_3BO_3. By altering the stoichiometry of LiOH, the reaction pathway was modified. Among all, the $LiBH_4$–3LiOH system demonstrated by far the most favourable attributes. The addition of $NiCl_2$ catalysed the system, resulting in a further significant decrease in the hydrogen desorption temperature from 220 °C to 80 °C. The $LiBH_4$–3LiOH and $LiBH_4$–3LiOH – 5 wt% $NiCl_2$ systems stand out not only for their impressive gravimetric capacity but also for their solid-state reactions at temperatures below 300 °C (below the melting temperature of reactants).

6. Future work

Reversibility of these systems is challenging due to the exothermic nature of the reactions. However, recent studies have explored the possibility of regenerating borohydride from borate end products. Zhu *et al.*[63] reported a cost-effective method to synthesize $Mg(BH_4)_2$ by converting B–O bonds to B–H bonds, achieved by milling MgH_2 with borates such as B_2O_3/$Mg(BO_2)_2$ to produce $Mg(BH_4)_2$. This process does not require high-pressure hydrogen but does necessitate the use of the expensive reducing agent MgH_2. Given that Li_3BO_3 and LiH are the primary reaction products in the $LiBH_4$–3LiOH system, exploring the potential to regenerate $LiBH_4$ by milling these end products without the need for an external reducing agent like MgH_2 or additional magnesium remains a significant and promising area for future research.

Also, Li_3BO_3 has several other important applications, such as being used as a CO_2 absorbent[64] or as an electrode material[65,66] in the battery industry. Investigating the potential to reuse this product or regenerate it could be an interesting avenue for future work to enhance the overall efficiency of the system.

Data availability

XRD data can be accessed from here: **https://figshare.com/s/a5919b638257530eac28**. Neutron data: neutron data id officially published in the ILL website and can be downloaded from: **https://doi.ill.fr/10.5291/ILL-DATA.1-04-185**.

Conflicts of interest

The authors declare that they have no known competing financial interests or personal relationships that could have appeared to influence the work reported in this paper.

Acknowledgements

This work was supported by the United Kingdom CDT programme – Fuel Cell & Their Fuels, hosted by University of Nottingham and funded by Engineering and Physical Sciences Research Council (EPSRC) (grant ref. EP/L015749/1) and Leverhulme Trust International Professorship Program (grant ref. LIP-2021-018). The authors extend their gratitude to Andrew Weilhard and David Furniss for their assistance with TPD-MS and FTIR studies, and to Saad Salman for reviewing the manuscript. We would also like to thank ILL France (exp no: doi.ill.fr/10.5291/ILL-DATA.1-04-185) for hosting us and helping us with the neutron experiment.

References

1 A. Züttel, P. Wenger, S. Rentsch, P. Sudan, P. Mauron and C. Emmenegger, $LiBH_4$ a new hydrogen storage material, *J. Power Sources*, 2003, **118**(1), 1–7, DOI: **10.1016/S0378-7753(03)00054-5**.

2 A. Züttel, S. Rentsch, P. Fischer, *et al.*, Hydrogen storage properties of $LiBH_4$, *J. Alloys Compd.*, 2003, **356–357**, 515–520, DOI: **10.1016/S0925-8388(02)01253-7**.

3 M. Paskevicius, L. H. Jepsen, P. Schouwink, *et al.*, Metal borohydrides and derivatives – synthesis, structure and properties, *Chem. Soc. Rev.*, 2017, **46**(5), 1565–1634, DOI: **10.1039/C6CS00705H**.

4 M. B. Ley, L. H. Jepsen, Y. S. Lee, *et al.*, Complex hydrides for hydrogen storage – new perspectives, *Mater. Today*, 2014, **17**(3), 122–128, DOI: **10.1016/j.mattod.2014.02.013**.

5 C. Milanese, S. Garroni, F. Gennari, *et al.*, Solid State Hydrogen Storage in Alanates and Alanate-Based Compounds: A Review, *Metals.*, 2018, **8**(8), 567, DOI: **10.3390/met8080567**.

6 K. Suárez-Alcántara, J. R. Tena-Garcia and R. Guerrero-Ortiz, Alanates, a Comprehensive Review, *Materials*, 2019, **12**, 2724, DOI: **10.3390/ma12172724**.

7 J. B. Eymery, S. Cahen, J. M. Tarascon and R. Janot, *Hydrogen storage by reaction between metallic amides and imides*, 2007, **https://www.osti.gov/etdeweb/biblio/21100402**.

8 H. Cao, Y. Zhang, J. Wang, Z. Xiong, G. Wu and P. Chen, Materials design and modification on amide-based composites for hydrogen storage, *Prog. Nat. Sci.: Mater. Int.*, 2012, **22**(6), 550–560, DOI: **10.1016/j.pnsc.2012.11.013**.

9 S. Qiu, H. Chu, Y. Zou, C. Xiang, F. Xu and L. Sun, Light metal borohydrides/amides combined hydrogen storage systems: composition, structure and properties, *J. Mater. Chem. A*, 2017, **5**(48), 25112–25130, DOI: **10.1039/C7TA09113C**.

10 C. C. Koch, Synthesis of nanostructured materials by mechanical milling: problems and opportunities, *Nanostruct. Mater.*, 1997, **9**(1), 13–22, DOI: **10.1016/S0965-9773(97)00014-7**.

11 L. Zaluski, A. Zaluska and J. O. Ström-Olsen, Nanocrystalline metal hydrides, *J. Alloys Compd.*, 1997, **253–254**, 70–79, DOI: **10.1016/S0925-8388(96)02985-4**.

12 J. Huot, G. Liang, S. Boily, A. Van Neste and R. Schulz, Structural study and hydrogen sorption kinetics of ball-milled magnesium hydride, *J. Alloys Compd.*, 1999, **293–295**, 495–500, DOI: 10.1016/S0925-8388(99)00474-0.

13 T. Das, S. Banerjee, K. Dasgupta, J. B. Joshi and V. Sudarsan, Nature of the Pd–CNT interaction in Pd nanoparticles dispersed on multi-walled carbon nanotubes and its implications in hydrogen storage properties, *RSC Adv.*, 2015, **5**(52), 41468–41474.

14 J. Mao, Z. Guo, X. Yu and H. Liu, Improved reversible dehydrogenation of $2LiBH_4 + MgH_2$ system by introducing Ni nanoparticles, *J. Mater. Res.*, 2011, **26**(9), 1143–1150.

15 H. Kou, X. Xiao, J. Li, *et al.*, Effects of fluoride additives on dehydrogenation behaviours of $2LiBH_4 + MgH_2$ system, *Int. J. Hydrogen Energy*, 2012, **37**(1), 1021–1026, DOI: 10.1016/j.ijhydene.2011.03.027.

16 J. J. Vajo and G. L. Olson, Hydrogen storage in destabilized chemical systems, *Scr. Mater.*, 2007, **56**(10), 829–834, DOI: 10.1016/j.scriptamat.2007.01.002.

17 A. F. Gross, J. J. Vajo, S. L. Van Atta and G. L. Olson, Enhanced Hydrogen Storage Kinetics of $LiBH_4$ in Nanoporous Carbon Scaffolds, *J. Phys. Chem. C*, 2008, **112**(14), 5651–5657, DOI: 10.1021/jp711066t.

18 *Solid-state hydrogen storage: materials and chemistry*, ed. G. Walker, Elsevier, 2008.

19 J. J. Vajo, S. L. Skeith and F. Mertens, Reversible Storage of Hydrogen in Destabilized $LiBH_4$, *J. Phys. Chem. B*, 2005, **109**(9), 3719–3722, DOI: 10.1021/jp040769o.

20 X. D. Kang, P. Wang, L. P. Ma and H. M. Cheng, Reversible hydrogen storage in $LiBH_4$ destabilized by milling with Al, *Appl. Phys. A: Solids Surf.*, 2007, **89**(4), 963–966, DOI: 10.1007/s00339-007-4198-z.

21 G. L. Xia, Y. H. Guo, Z. Wu and X. B. Yu, Enhanced hydrogen storage performance of $LiBH_4$–Ni composite, *J. Alloys Compd.*, 2009, **479**(1), 545–548, DOI: 10.1016/j.jallcom.2008.12.128.

22 J. Yang, A. Sudik and C. Wolverton, Destabilizing $LiBH_4$ with a Metal (M = Mg, Al, Ti, V, Cr, or Sc) or Metal Hydride (MH_2 = MgH_2, TiH_2, or CaH_2), *J. Phys. Chem. C*, 2007, **111**(51), 19134–19140, DOI: 10.1021/jp076434z.

23 J. H. Shim, J. H. Lim, R. S. ullah, *et al.*, Effect of Hydrogen Back Pressure on Dehydrogenation Behaviour of $LiBH_4$-Based Reactive Hydride Composites, *J. Phys. Chem. Lett.*, 2010, **1**(1), 59–63, DOI: 10.1021/jz900012n.

24 D. M. Liu, W. J. Huang, T. Z. Si and Q. A. Zhang, Hydrogen storage properties of $LiBH_4$ destabilized by SrH_2, *J. Alloys Compd.*, 2013, **551**, 8–11, DOI: 10.1016/j.jallcom.2012.09.138.

25 T. E. C. Price, D. M. Grant, V. Legrand and G. S. Walker, Enhanced kinetics for the $LiBH_4 : MgH_2$ multi-component hydrogen storage system – The effects of stoichiometry and decomposition environment on cycling behaviour, *Int. J. Hydrogen Energy*, 2010, **35**(9), 4154–4161, DOI: 10.1016/j.ijhydene.2010.02.082.

26 G. Barkhordarian, T. Klassen, M. Dornheim and R. Bormann, Unexpected kinetic effect of MgB_2 in reactive hydride composites containing complex borohydrides, *J. Alloys Compd.*, 2007, **440**(1), L18–L21, DOI: 10.1016/j.jallcom.2006.09.048.

27 M. Au, W. Spencer, A. Jurgensen and C. Zeigler, Hydrogen storage properties of modified lithium borohydrides, *J. Alloys Compd.*, 2008, **462**(1), 303–309, DOI: 10.1016/j.jallcom.2007.08.044.

28 Y. Zhang, W. S. Zhang, M. Q. Fan, *et al.*, Enhanced Hydrogen Storage Performance of $LiBH_4$–SiO_2–TiF_3 Composite, *J. Phys. Chem. C*, 2008, **112**(10), 4005–4010, DOI: 10.1021/jp709814b.

29 X. B. Yu, D. M. Grant and G. S. Walker, Low-Temperature Dehydrogenation of $LiBH_4$ through Destabilization with TiO_2, *J. Phys. Chem. C*, 2008, **112**(29), 11059–11062, DOI: 10.1021/jp800602d.

30 M. Meggouh, D. M. Grant, O. Deavin, M. Brunelli, T. C. Hansen and G. S. Walker, Investigation of the dehydrogenation behavior of the $2LiBH_4 : CaNi_5$ multicomponent hydride system, *Int. J. Hydrogen Energy*, 2015, **40**(7), 2989–2996, DOI: 10.1016/j.ijhydene.2014.12.059.

31 P. Chen, Z. Xiong, J. Luo, J. Lin and K. L. Tan, Interaction between Lithium Amide and Lithium Hydride, *J. Phys. Chem. B*, 2003, **107**(39), 10967–10970, DOI: 10.1021/jp034149j.

32 Y. Guo, G. Xia, Y. Zhu, L. Gao and X. Yu, Hydrogen release from ammine lithium borohydride, $LiBH_4 \cdot NH_3$, *Chem. Commun.*, 2010, **46**(15), 2599–2601.

33 J. Luo, H. Wu, W. Zhou, X. Kang, Z. Fang and P. Wang, $LiBH_4 \cdot NH_3BH_3$: a new lithium borohydride ammonia borane compound with a novel structure and favourable hydrogen storage properties, *Int. J. Hydrogen Energy*, 2012, **37**(14), 10750–10757, DOI: 10.1016/j.ijhydene.2012.04.049.

34 T. He, H. Wu, G. Wu, *et al.*, Borohydride hydrazinates: high hydrogen content materials for hydrogen storage, *Energy Environ. Sci.*, 2012, **5**(2), 5686–5689.

35 W. Cai, H. Wang, D. Sun, Q. Zhang, X. Yao and M. Zhu, Destabilization of $LiBH_4$ dehydrogenation through H^+–H^- interactions by cooperating with alkali metal hydroxides, *RSC Adv.*, 2014, **4**(6), 3082–3089, DOI: 10.1039/C3RA45847D.

36 Ü. I. B. I. DEMIRCI, Sodium borohydride for the near-future energy: a "rough diamond" for Turkey, *Turk. J. Chem.*, 2018, **42**(2), 193–220.

37 J. P. Goudon, F. Bernard, J. Renouard and P. Yvart, Experimental investigation on lithium borohydride hydrolysis, *Int. J. Hydrogen Energy*, 2010, **35**(20), 11071–11076, DOI: 10.1016/j.ijhydene.2010.07.023.

38 L. Laversenne, C. Goutaudier, R. Chiriac, C. Sigala and B. Bonnetot, Hydrogen storage in borohydrides comparison of hydrolysis conditions of $LiBH_4$, $NaBH_4$ and KBH_4, *J. Therm. Anal. Calorim.*, 2008, **94**, 785–790.

39 J. J. Vajo, S. L. Skeith, F. Mertens and S. W. Jorgensen, Hydrogen-generating solid-state hydride/hydroxide reactions, *J. Alloys Compd.*, 2005, **390**(1), 55–61, DOI: 10.1016/j.jallcom.2004.08.042.

40 Y. Liu, Y. Zhang, H. Zhou, Y. Zhang, M. Gao and H. Pan, Reversible hydrogen storage behaviour of $LiBH_4$–$Mg(OH)_2$ composites, *Int. J. Hydrogen Energy*, 2014, **39**(15), 7868–7875, DOI: 10.1016/j.ijhydene.2014.03.137.

41 J. M. Kiat, G. Boemare, B. Rieu and D. Aymes, Structural evolution of LiOH: evidence of a solid–solid transformation toward Li_2O close to the melting temperature, *Solid State Commun.*, 1998, **108**(4), 241–245, DOI: 10.1016/S0038-1098(98)00346-9.

42 H. Kou, G. Sang, Y. Zhou, *et al.*, Enhanced hydrogen storage properties of $LiBH_4$ modified by NbF_5, *Int. J. Hydrogen Energy*, 2014, **39**(22), 11675–11682, DOI: 10.1016/j.ijhydene.2014.05.179.

43 C. Zhou, J. B. Grinderslev, L. N. Skov, *et al.*, Polymorphism, ionic conductivity and electrochemical properties of lithium closo-deca-and dodeca-borates and their composites, $Li_2B_{10}H_{10}$–$Li_2B_{12}H_{12}$, *J. Mater. Chem. A*, 2022, **10**(30), 16137–16151.

44 M. P. Pitt, M. Paskevicius, D. H. Brown, D. A. Sheppard and C. E. Buckley, Thermal stability of $Li_2B_{12}H_{12}$ and its role in the decomposition of $LiBH_4$, *J. Am. Chem. Soc.*, 2013, **135**(18), 6930–6941.

45 J. Zhu, Y. Mao, H. Wang, J. Liu, L. Ouyang and M. Zhu, Reaction Route Optimized $LiBH_4$ for High Reversible Capacity Hydrogen Storage by Tunable Surface-Modified AlN, *ACS Appl. Energy Mater.*, 2020, **3**(12), 11964–11973, DOI: 10.1021/acsaem.0c02140.

46 C. C. Zhang, X. Gao and B. Yilmaz, Development of FTIR Spectroscopy Methodology for Characterization of Boron Species in FCC Catalysts, *Catalysts*, 2020, **10**(11), 1327, DOI: 10.3390/catal10111327.

47 R. Ren, A. L. Ortiz, T. Markmaitree, W. Osborn and L. L. Shaw, Stability of Lithium Hydride in Argon and Air, *J. Phys. Chem. B*, 2006, **110**(21), 10567–10575, DOI: 10.1021/jp060068m.

48 B. J. Zhang and B. H. Liu, Hydrogen desorption from $LiBH_4$ destabilized by chlorides of transition metal Fe, Co, and Ni, *Int. J. Hydrogen Energy*, 2010, **35**(14), 7288–7294, DOI: 10.1016/j.ijhydene.2010.04.165.

49 W. S. Tang, G. Wu, T. Liu, *et al.*, Cobalt-catalyzed hydrogen desorption from the $LiNH_2$–$LiBH_4$ system, *Dalton Trans.*, 2008, **18**, 2395–2399, DOI: 10.1039/B719420J.

50 M. Sweta, G. David and T. Hansen, Neutron Diffraction Study for $LiBH_4$–LiOH System as a Hydrogen Storage, *Materials*, 2021, DOI: 10.5291/ILL-DATA.1-04-185.

51 S. Mondal and A. K. Banthia, Low-temperature synthetic route for boron carbide, *J. Eur. Ceram. Soc.*, 2005, **25**(2), 287–291, DOI: 10.1016/j.jeurceramsoc.2004.08.011.

52 E. Betourne and M. Touboul, Crystallographic data about hydrated and anhydrous lithium monoborates, *Powder Diffr.*, 1997, **12**(3), 155–159.

53 E. Petit, F. Salles, D. Alligier and U. B. Demirci, Hydrolysis of the Borohydride Anion BH_4^-: A ^{11}B NMR Study Showing the Formation of Short-Living Reaction Intermediates including BH_3OH^-, *Molecules*, 2022, **27**(6), 1975.

54 N. Koga and T. Utsuoka, Thermal dehydration of lithium metaborate dihydrate and phase transitions of anhydrous product, *Thermochim. Acta*, 2006, **443**(2), 197–205.

55 R. P. Awbery, D. A. Broughton and S. C. Tsang, In situ observation of lithium hydride hydrolysis by DRIFT spectroscopy, *J. Nucl. Mater.*, 2008, **373**(1), 94–102, DOI: 10.1016/j.jnucmat.2007.05.039.

56 K. Chen, L. Ouyang, H. Wang, J. Liu, H. Shao and M. Zhu, A high-performance hydrogen generation system: Hydrolysis of $LiBH_4$-based materials catalysed by transition metal chlorides, *Renewable Energy*, 2020, **156**, 655–664, DOI: 10.1016/j.renene.2020.04.030.

57 G. Rousse, B. Baptiste and G. Lelong, Crystal structures of $Li_6B_4O_9$ and $Li_3B_{11}O_{18}$ and application of the dimensional reduction formalism to lithium borates, *Inorg. Chem.*, 2014, **53**(12), 6034–6041.

58 X. B. Yu, D. M. Grant and G. S. Walker, A new dehydrogenation mechanism for reversible multicomponent borohydride systems—the role of Li–Mg alloys, *Chem. Commun.*, 2006, (37), 3906–3908.

59 J. J. Vajo, S. L. Skeith and F. Mertens, Reversible storage of hydrogen in destabilized $LiBH_4$, *J. Phys. Chem. B*, 2005, **109**(9), 3719–3722.

60 P. Mauron, M. Bielmann, A. Remhof, A. Züttel, J. H. Shim and Y. W. Cho, Stability of the $LiBH_4/CeH_2$ composite system determined by dynamic PCT measurements, *J. Phys. Chem. C*, 2010, **114**(39), 16801–16805.

61 A. Ibikunle, A. J. Goudy and H. Yang, Hydrogen storage in a $CaH_2/LiBH_4$ destabilized metal hydride system, *J. Alloys Compd.*, 2009, **475**(1), 110–115, DOI: 10.1016/j.jallcom.2008.08.010.

62 Y. Li, P. Li and X. Qu, Investigation on $LiBH_4$–CaH_2 composite and its potential for thermal energy storage, *Sci. Rep.*, 2017, **7**(1), 41754, DOI: 10.1038/srep41754.

63 Y. Zhu, S. Shen, L. Ouyang, *et al.*, Effective synthesis of magnesium borohydride *via* B–O to B–H bond conversion, *Chem. Eng. J.*, 2022, **432**, 134322, DOI: 10.1016/j.cej.2021.134322.

64 T. Harada and T. A. Hatton, Tri-lithium borate (Li_3BO_3); a new highly regenerable high capacity CO_2 adsorbent at intermediate temperature, *J. Mater. Chem. A*, 2017, **5**(42), 22224–22233, DOI: 10.1039/C7TA06167F.

65 E. Il'ina, S. Pershina, B. Antonov and A. Pankratov, Impact of Li_3BO_3 addition on solid electrode-solid electrolyte interface in all-solid-state batteries, *Materials*, 2021, **14**(22), 7099, DOI: 10.3390/ma14227099.

66 M. Zhang, M. Zhu, W. Dai, *et al.*, Surface coating with Li_3BO_3 protection layer to enhance the electrochemical performance and safety properties of Ni-rich $LiNi_{0.85}Co_{0.05}Mn_{0.10}O_2$ cathode material, *Powder Technol.*, 2021, **394**, 448–458, DOI: 10.1016/j.powtec.2021.08.083.

